

## Measurement of Acoustic Velocity in Poly(methyl methacrylate)-Based Polymer Optical Fiber for Brillouin Frequency Shift Estimation

Neisei Hayashi, Yosuke Mizuno, Daisuke Koyama, and Kentaro Nakamura

*Precision and Intelligence Laboratory, Tokyo Institute of Technology, Yokohama 226-8503, Japan*

Received August 1, 2011; accepted August 27, 2011; published online September 14, 2011

The acoustic velocity in a poly(methyl methacrylate) (PMMA) polymer optical fiber (POF) was measured to be  $2.8 \times 10^3$  m/s using ultrasonic pulse-echo technique, from which its Brillouin frequency shift (BFS) was estimated to be  $\sim 13$  GHz at 650 nm. The BFS was also predicted to show a negative dependence on temperature with a coefficient of approximately  $-17.1$  MHz/K at 650 nm,  $-14.5$  times larger than that of a silica fiber at  $1.55 \mu\text{m}$ . © 2011 The Japan Society of Applied Physics

Brillouin scattering in optical fibers has been widely studied,<sup>1,2)</sup> and has various applications, such as lasing,<sup>2)</sup> slow light generation,<sup>3)</sup> core alignment of butt coupling,<sup>4)</sup> strain/temperature sensing,<sup>5-7)</sup> and many others. To improve their performance, Brillouin scattering not only in standard silica-based optical fibers but also in some specialty fibers, including tellurite glass fibers,<sup>8,9)</sup> bismuth-oxide fibers,<sup>10,11)</sup> and photonic crystal fibers,<sup>12,13)</sup> has been vigorously studied so far. Recently, we have succeeded in observing Brillouin scattering in perfluorinated graded-index polymer optical fibers (PFGI-POFs)<sup>14,15)</sup> at  $1.55 \mu\text{m}$ , which offer extremely high flexibility, easy and low-cost connection, and high safety compared with other standard glass fibers.<sup>16)</sup> The Brillouin frequency shift (BFS) was 2.83 GHz, and the Brillouin gain coefficient was estimated to be  $3.09 \times 10^{-11}$  m/W, which was almost the same as that of a silica single-mode fiber (SMF). This result indicates that Brillouin scattering in PFGI-POFs can be applied to a variety of practical devices and systems in the same way as that in silica SMFs. We have also investigated the dependences of the BFS on strain and temperature in the PFGI-POF at  $1.55 \mu\text{m}$ , and found that Brillouin scattering in PFGI-POFs has a big potential for use in the development of high-precision temperature sensors with reduced strain sensitivity.<sup>17)</sup> However, Brillouin scattering in standard poly(methyl methacrylate) (PMMA)-based POFs has not been experimentally observed yet for the following two reasons: (1) it is difficult to develop a Brillouin monitoring system including an optical amplifier, optical circulator, etc., at 650 nm, where the propagation loss is minimal, and (2) their core diameter is so large (typically  $980 \mu\text{m}$ ) that the Brillouin threshold power is extremely high. We believe that clarification of the Brillouin scattering properties in PMMA-POFs is as significant as that in PFGI-POFs, since PMMA-POFs are much more cost-effective and more widely used in communication applications.

In this paper, we measure the acoustic velocity in POFs using ultrasonic pulse-echo technique, and estimate their BFSs. First, in order to confirm the validity of this method, we show that the estimated BFS of a PFGI-POF of  $\sim 2.9$  GHz at  $1.55 \mu\text{m}$  moderately agrees with the actual value previously reported. Then, we measure the acoustic velocity in a PMMA-POF with a  $980 \mu\text{m}$  core diameter to be  $2.8 \times 10^3$  m/s, from which its BFS is estimated to be  $\sim 5.4$  GHz at  $1.55 \mu\text{m}$  and  $\sim 13$  GHz at 650 nm. Finally, we estimate the coefficient of the temperature dependence of the BFS in a PMMA-POF to be  $-7.2$  MHz/K at  $1.55 \mu\text{m}$  and  $-17$  MHz/K at 650 nm, which are  $-6.1$  and  $-14.5$

times larger than that of a silica fiber at  $1.55 \mu\text{m}$ , respectively.

When pump light is injected into an optical fiber, backscattered light, also called Stokes light, is generated due to the interaction with acoustic phonons, and it propagates in the direction opposite to the pump light. This phenomenon is called spontaneous Brillouin scattering. The Brillouin-scattered light spectrum, also known as Brillouin gain spectrum (BGS), takes the shape of a Lorentzian function.<sup>2)</sup> The frequency at which the peak power is obtained in the spectrum is downshifted by several GHz from the incident light frequency, and the amount of this frequency shift is known as BFS. When the pump light wavelength is  $1.55 \mu\text{m}$ , the amounts of BFS are reported to be  $\sim 10.8$  GHz for silica-based SMFs<sup>2)</sup> and  $\sim 2.83$  GHz for PFGI-POFs.<sup>14)</sup> In optical fibers, the BFS  $\nu_B$  is given as<sup>2)</sup>

$$\nu_B = \frac{2nv_A}{\lambda_p}, \quad (1)$$

where  $n$  is the refractive index,  $v_A$  is the acoustic velocity in the fiber, and  $\lambda_p$  is the wavelength of the incident pump light. Thus, we can estimate the BFS using the value of  $v_A$ . If either tensile strain or temperature changes in standard silica SMFs, the BFS moves to higher frequency in proportion to the applied strain ( $+580$  MHz/%)<sup>18)</sup> or temperature change ( $+1.18$  MHz/K).<sup>19)</sup> In PFGI-POFs, the BFS is known to move to lower frequency with increasing applied strain ( $-121.8$  MHz/%)<sup>17)</sup> or temperature ( $-4.09$  MHz/K).<sup>17)</sup> In both cases, by measuring the BFS in the fibers, the strain amplitude or temperature change can be derived.

We employed two kinds of POF samples. One was a PFGI-POF with numerical aperture (NA) of 0.185, core diameter of  $120 \mu\text{m}$ , cladding diameter of  $490 \mu\text{m}$ , core refractive index of  $\sim 1.35$ , and propagation losses of  $\sim 150$  dB/km at  $1.55 \mu\text{m}$  and  $\sim 100$  dB/km at 650 nm. The other sample was a PMMA-POF with NA of 0.5, core diameter of  $980 \mu\text{m}$ , cladding diameter of  $1000 \mu\text{m}$ , core refractive index of  $\sim 1.49$ , and propagation loss of  $\sim 150$  dB/km at 650 nm (extremely high loss at  $1.55 \mu\text{m}$ ). The lengths of the PFGI-POF and PMMA-POF were 4.2 and 3.9 mm as shown in Figs. 1(a) and 1(b), respectively. The entire measurement setup is depicted in Fig. 2. The ultrasonic pulse generated with an unfocused transducer (Panametrics M316) connected to a pulser-receiver (Panametrics 5900PR) was directed to the POF samples fixed in degassed water, and the reflected wave was received with the same transducer. The center frequency of the pulse was 10.0 MHz, and the diameter of the ultrasonic beam was 3.2 mm. The magnified

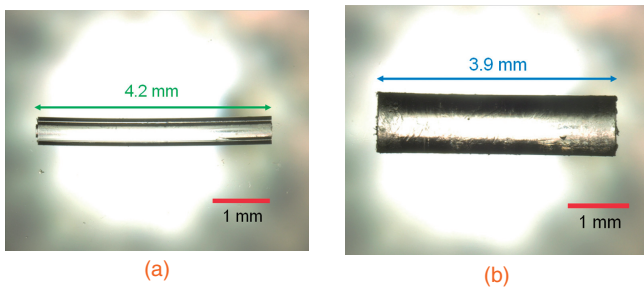


**Fig. 1.** Microscope images of (a) the PFGI-POF sample and (b) the PMMA-POF sample.

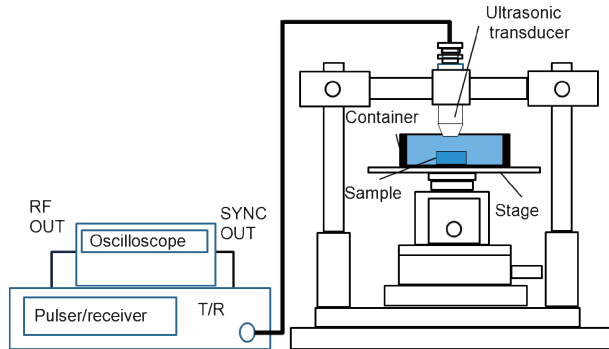


**Fig. 2.** Entire experimental setup for measuring the acoustic velocity in POFs.

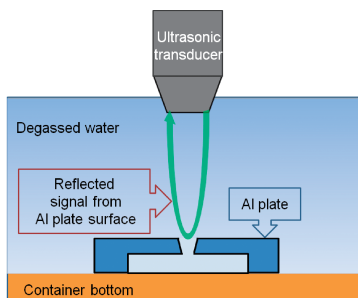


**Fig. 3.** Schematic setup without the POF samples.

view around the transducer when the POF samples were not employed is schematically shown in Fig. 3. The aluminum (Al) plate had a hole of  $\sim 1$  mm diameter to fix the PMMA-POF. The magnified views with the PFGI- and PMMA-POF samples employed are depicted in Figs. 4(a) and 4(b), respectively. The PFGI-POF was perpendicularly placed on the Al plate, while the PMMA-POF was fixed perpendicularly to the Al plate by making use of the hole.

Figure 5(a) shows the measured echo waveform without the POF sample. The first signal, where the time delay  $t$  was defined as  $0 \mu\text{s}$ , represents the launched wave. Several large peaks observed at  $t > 11.8 \mu\text{s}$  are due to the reflection from the Al plate. The first peak (A) at  $t \sim 11.8 \mu\text{s}$  and the second peak (B) at  $t \sim 12.4 \mu\text{s}$  correspond to the reflected waves at the surface and bottom of the Al plate, respectively. Other peaks (C) following them at  $t > 13.0 \mu\text{s}$  are due to the multiple reflection in the Al plate. Figure 5(b) shows the measured echo waveform with the 4.2 mm PFGI-POF sample employed. By comparing Figs. 5(a) and 5(b),

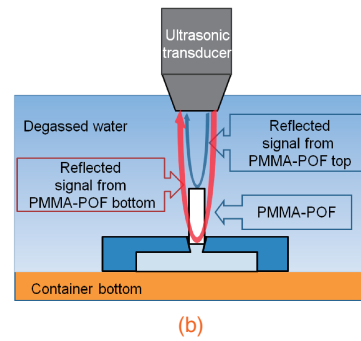
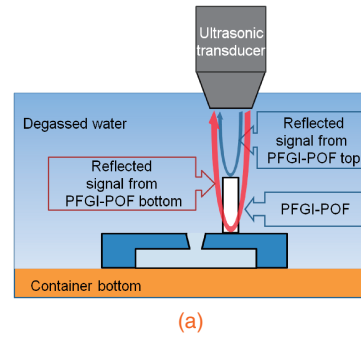


**Fig. 4.** Schematic setups (a) with the PFGI-POF sample and (b) with the PMMA-POF sample.

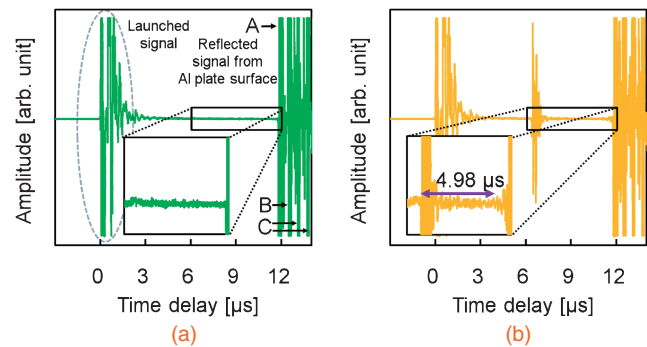


**Fig. 5.** Measured echo waveforms (a) without and (b) with the PFGI-POF sample.

we know that the two peaks at  $t \sim 6.4 \mu\text{s}$  and at  $t \sim 11.4 \mu\text{s}$  correspond to the reflected waves at the surface and bottom of the PFGI-POF, respectively. The peak at  $t \sim 11.4 \mu\text{s}$  was much smaller than the peak (A) at  $t \sim 11.8 \mu\text{s}$  because of the small core area and low acoustic reflectivity of the PFGI-POF/water boundary compared with those of the water/Al boundary. From the magnified view around these two peaks, the exact time delay was found to be  $4.98 \mu\text{s}$ , and the acoustic velocity  $v_A$  was calculated to be  $\sim 1.7 \times 10^3$  m/s. By substituting this value in eq. (1), with the pump wavelength of  $1.55 \mu\text{m}$ , its BFS was estimated to be approximately 2.9 GHz, which is in moderate agreement with the previously reported value of 2.83 GHz.<sup>14)</sup> Though this discrepancy seems to be caused by the insufficient resolution in calculating  $v_A$ , it was shown that this method can be used to roughly estimate the BFS. When the pump wavelength was  $650$  nm, where the propagation loss in PMMA-POFs is minimal, the BFS in the PFGI-POF was estimated to be approximately 7.0 GHz.

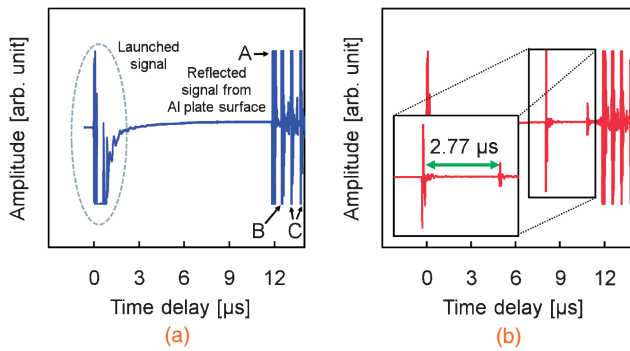


Fig. 6. Measured echo waveforms (a) without and (b) with the PMMA-POF sample.

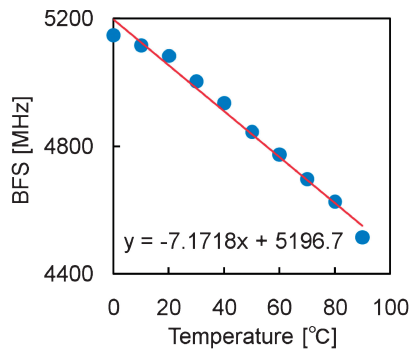


Fig. 7. BFS dependence on temperature in PMMA-POF at 1.55  $\mu\text{m}$ , estimated using the data in ref. 20.

Next, we measured the acoustic velocity in the PMMA-POF and estimated its BFS. Figure 6(a) shows the measured echo waveform without the PMMA-POF sample, which can be interpreted in the same way as Fig. 5(a). The positions of the peaks (A, B, and C) differed from those in Fig. 5(a), because the vertical position of the transducer was slightly lower. The measured echo waveform with the 3.9 mm PMMA-POF sample employed is shown in Fig. 6(b). By comparing Figs. 6(a) and 6(b), it is clear that the two peaks at  $t \sim 8 \mu\text{s}$  and at  $t \sim 11 \mu\text{s}$  correspond to the reflected waves at the surface and bottom of the PMMA-POF, respectively. The exact time delay was measured to be  $2.77 \mu\text{s}$ , and the acoustic velocity  $v_A$  in the PMMA-POF was calculated to be  $2.8 \times 10^3 \text{ m/s}$ , which is nearly comparable to the acoustic velocity of  $2644 (\pm 25) \text{ m/s}$  in bulk PMMA.<sup>20</sup> Its BFS at 650 nm was also estimated to be  $\sim 13 \text{ GHz}$ , which is close to  $\sim 11 \text{ GHz}$  of silica fibers at 1.55  $\mu\text{m}$ .<sup>2)</sup> In contrast, its BFS at 1.55  $\mu\text{m}$  was estimated to be  $\sim 5.4 \text{ GHz}$ , which is about twice of 2.83 GHz in PFGI-POFs at 1.55  $\mu\text{m}$ .<sup>14)</sup>

Since the measured acoustic velocity in the PMMA-POF was close to that in bulk PMMA, we can estimate the temperature dependence of the BFS in the PMMA-POF using the data in ref. 20, where acoustic velocities in bulk PMMA at each temperature from 0 to 90  $^\circ\text{C}$  are provided. The estimated BFS dependence on temperature in PMMA-POF at 1.55  $\mu\text{m}$  is shown in Fig. 7. We can see that the temperature coefficient is approximately  $-7.2 \text{ MHz/K}$ , the absolute value of which is 6.1 and 1.8 times larger than those of a silica fiber ( $+1.18 \text{ MHz/K}$ <sup>19)</sup> and a PFGI-POF

( $-4.09 \text{ MHz/K}$ <sup>17)</sup>) at 1.55  $\mu\text{m}$ , respectively. On the other hand, when the pump wavelength is 650 nm, the coefficient is calculated to be as large as  $-17.1 \text{ MHz/K}$ . The larger temperature coefficient leads to precision enhancement of the temperature measurement, and consequently, the Brillouin scattering in the PMMA-POF can be potentially utilized to develop high-precision temperature sensors.

In conclusion, the acoustic velocities in POFs were measured based on the ultrasonic pulse-echo technique for the estimation of their BFS. First, the BFS of a PFGI-POF at 1.55  $\mu\text{m}$  was estimated to be  $\sim 2.9 \text{ GHz}$ . This value moderately agreed with the actual value previously reported, indicating that this method can be used to roughly estimate the BFS. Then, the acoustic velocity in a PMMA-POF with 980  $\mu\text{m}$  core diameter was measured to be  $2.8 \times 10^3 \text{ m/s}$ , from which its BFS was estimated to be  $\sim 13 \text{ GHz}$  at 650 nm and  $\sim 5.4 \text{ GHz}$  at 1.55  $\mu\text{m}$ . In addition, the coefficient of the temperature dependence of the BFS in a PMMA-POF was estimated to be  $-7.2 \text{ MHz/K}$  at 1.55  $\mu\text{m}$  and  $-17.1 \text{ MHz/K}$  at 650 nm, which are  $-6.1$  times and  $-14.5$  times larger than that of a silica fiber at 1.55  $\mu\text{m}$ , respectively. We expect that this information will be a useful guideline for observing and exploiting Brillouin scattering in PMMA-POFs for various applications in the future including distributed Brillouin sensors with low cost and robustness. The experimental observation of Brillouin scattering in PMMA-POFs might be feasible by employing high-power visible light, at the wavelength of which their propagation loss is minimum.

**Acknowledgments** The authors are indebted to the staff of the Technical Department, Tokyo Institute of Technology, for providing the Al plate used in the experiment. The work of Y. Mizuno was supported by the Research Fellowships for Young Scientists from the Japan Society for the Promotion of Science (JSPS).

- 1) E. P. Ippen and R. H. Stolen: *Appl. Phys. Lett.* **21** (1972) 539.
- 2) G. P. Agrawal: *Nonlinear Fiber Optics* (Academic Press, San Diego, CA, 2001) Chap. 3.
- 3) K. Y. Song, M. G. Herraes, and L. Thevenaz: *Opt. Express* **13** (2005) 82.
- 4) Y. Mizuno and K. Nakamura: *J. Lightwave Technol.* **29** (2011) 2616.
- 5) T. Horiguchi and M. Tateda: *J. Lightwave Technol.* **7** (1989) 1170.
- 6) K. Hotate and T. Hasegawa: *IEICE Trans. Electron.* **E83-C** (2000) 405.
- 7) Y. Mizuno, W. Zou, Z. He, and K. Hotate: *Opt. Express* **16** (2008) 12148.
- 8) K. S. Abedin: *Opt. Express* **14** (2006) 11766.
- 9) Y. Mizuno, Z. He, and K. Hotate: *Opt. Commun.* **283** (2010) 2438.
- 10) J. H. Lee, T. Tanemura, K. Kikuchi, T. Nagashima, T. Hasegawa, S. Ohara, and N. Sugimoto: *Opt. Lett.* **30** (2005) 1698.
- 11) Y. Mizuno, Z. He, and K. Hotate: *Appl. Phys. Express* **2** (2009) 112402.
- 12) J. H. Lee, Z. Yusoff, W. Belardi, M. Ibsen, T. M. Monro, and D. J. Richardson: *Opt. Lett.* **27** (2002) 927.
- 13) J. C. Beugnot, T. Sylvestre, D. Alasia, H. Maillotte, V. Laude, A. Monteville, L. Provino, N. Traynor, S. F. Mafang, and L. Thevenaz: *Opt. Express* **15** (2007) 15517.
- 14) Y. Mizuno and K. Nakamura: *Appl. Phys. Lett.* **97** (2010) 021103.
- 15) T. Ishigure, Y. Koike, and J. W. Fleming: *J. Lightwave Technol.* **18** (2000) 178.
- 16) M. G. Kuzyk: *Polymer Fiber Optics: Materials, Physics, and Applications* (CRC Press, Boca Raton, FL, 2006).
- 17) Y. Mizuno and K. Nakamura: *Opt. Lett.* **35** (2010) 3985.
- 18) T. Horiguchi, T. Kurashima, and M. Tateda: *IEEE Photonics Technol. Lett.* **1** (1989) 107.
- 19) T. Kurashima, T. Horiguchi, and M. Tateda: *Appl. Opt.* **29** (1990) 2219.
- 20) J. Saneyoshi, Y. Kikuchi, and O. Nomoto: *Cho-onpa Gijutsu Binran* (Handbook of Ultrasonic Technology) (Nikkan Kogyo, Tokyo, 1978) p. 1353.